

AN X-RAY STUDY OF THE SUPERNOVA REMNANT G290.1–0.8

PATRICK SLANE¹, RANDALL K. SMITH¹, JOHN P. HUGHES², AND ROBERT PETRE³

For Publication in The Astrophysical Journal: Accepted 28 August 2001

ABSTRACT

G290.1–0.8 (MSH 11–61A) is a supernova remnant (SNR) whose X-ray morphology is centrally bright. However, unlike the class of X-ray composite SNRs whose centers are dominated by nonthermal emission, presumably driven by a central pulsar, we show that the X-ray emission from G290.1–0.8 is thermal in nature, placing the remnant in an emerging class which includes such remnants as W44, W28, 3C391, and others. The evolutionary sequence which leads to such X-ray properties is not well understood. Here we investigate two scenarios for such emission: evolution in a cloudy interstellar medium, and early-stage evolution of a remnant into the radiative phase, including the effects of thermal conduction. We construct models for these scenarios in an attempt to reproduce the observed center-filled X-ray properties of G290.1–0.8, and we derive the associated age, energy, and ambient density conditions implied by the models. We find that for reasonable values of the explosion energy, the remnant age is of order $(1-2) \times 10^4$ yr. This places a fairly strong constraint on any association between G290.1–0.8 and PSR J1105-610, which would require an anomalously large velocity for the pulsar.

Subject headings: ISM: individual (G290.1–0.8/MSH 11–61A) — supernova remnants — X-rays: interstellar

1. INTRODUCTION

A distinct subset of moderate age supernova remnants (SNRs) are characterized by an X-ray morphology which is centrally brightened, in contrast to a more limb-brightened radio profile. In some cases (e.g. CTA 1 [Slane et al. 1997], MSH 11–62 [Harrus, Hughes, & Slane 1998], G39.2–0.1 [Harrus & Slane 1999]) recent observations have shown that the central emission is nonthermal in nature, presumably associated with a pulsar-driven synchrotron nebula. For others, however, the central emission is decidedly thermal (e.g. W44 [Jones, Smith & Angellini 1993]; 3C391 [Rho & Petre 1996, Chen & Slane 2001]; G272.2–3.2 [Harrus et al. 2001]). A recent list of the members of this “mixed morphology” class of SNRs has been compiled by Rho & Petre (1998). The evolutionary characteristics which have led to such an observed profile are not well understood. One possible scenario is that the shells in these remnants have recently become radiative, thus leaving only the hot interior to persist in X-rays (Smith et al. 1985, Harrus et al. 1997), a picture that is enhanced by the effects of thermal conduction on the temperature and density distribution in the SNR (Cox et al. 1999). Another suggestion is that the central emission measure has been enhanced by the presence of cool clouds left relatively intact after the passage of the blast wave to slowly evaporate in the hot SNR interior (Cowie & McKee 1977, McKee & Ostriker 1977, White & Long 1991).

Early X-ray observations with the *Einstein* Observatory (Seward 1990) established the center-filled nature of the X-ray emission from G290.1–0.8. However, the spectral characteristics of the remnant are poorly constrained by these data, leaving open the question of whether the centrally enhanced X-ray emission is thermal or nonthermal in nature. The remnant was not observed with the ROSAT PSPC. Optical observations of the remnant show patchy emission with an enhanced [S II]/H α ratio typical of SNRs (Kirshner & Winkler 1979, Elliott & Malin 1979). In the radio band (Figure 1) G290.1–0.8 is classified

as a shell-type SNR (Green 1998) although the morphology is actually somewhat “plateau-like” with the exception of a partial shell along the western limb along with other patchy structures interior to the SNR boundary (Whiteoak & Green 1996). The remnant is $10' \times 14'$ in size, distinctly elongated in the southeast-northwest direction. This is roughly aligned with the Galactic plane, much like other “bilateral” SNRs whose morphologies may be the result of magnetic field structures near the plane (Gaensler 1998). A young pulsar (J1105-6107) has been discovered nearby the SNR (Kaspi et al. 1997). Its location is well outside the remnant, along the axis of elongation (and outside the field of view in Figure 1). The spin-down age of the pulsar is ~ 60 kyr, considerably larger than the expected age for a remnant which is still X-ray luminous. Moreover, as pointed out by Kaspi et al. (1997), the age is even larger for a braking index $n < 3$, which may be more typical of pulsars. These standard calculations assume that the current spin period P is much longer than the initial period P_0 (i.e. that the pulsar has spun down considerably since birth). Relaxing this constraint can lead to an inferred pulsar age that is consistent with that of the remnant. We discuss constraints on the association of J1105-6107 with G290.1–0.8 in Section 4 below.

The distance to G290.1–0.8 is not well known. H I measurements (Goss et al. 1972, Dickel 1973) show absorption out to $V_{LSR} \sim -25$ km s^{–1} indicating that the remnant lies beyond the tangent point with $D > 2.9$ kpc. Fabry-Perot measurements of the H α line (Rosado et al. 1996) appear to show an emission component at $V_{LSR} \sim +12$ km s^{–1} associated with the SNR, indicating a distance $D = 6.9$ kpc. The emission is weak, however, and the H α emission is quite complex in this region. The H I profiles from Goss et al. (1972) indicate absorption at positive velocities as well, but those measured by Dickel (1973) do not. Finally, based upon a relatively low observed S II/H α ratio (~ 0.5), Elliot & Malin (1979) argue that G290.1–0.8 is a large, old remnant which, given its angular size, could be at a distance of $\sim 12-14$ kpc. However, studies of the S II/H α ra-

¹Harvard-Smithsonian Center for Astrophysics, 60 Garden Street, Cambridge, MA 02138

²Department of Physics and Astronomy, Rutgers, The State University of New Jersey, 136 Frelinghuysen Road, Piscataway, NJ 08854-8019

³Laboratory for High Energy Astrophysics, Goddard Space Flight Center, Baltimore, MD 20771

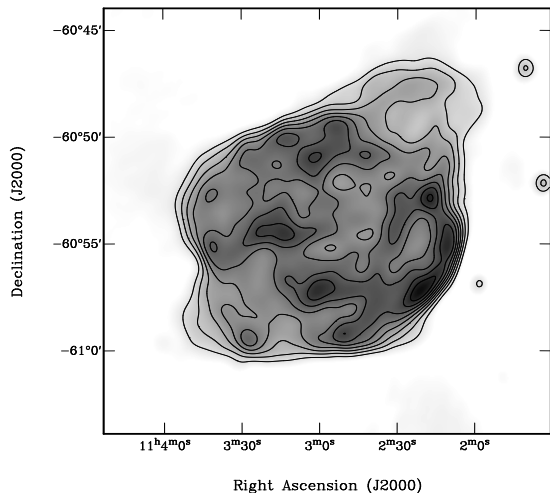


FIG. 1.— Radio continuum image (843 MHz) of G290.1–0.8 from MOST (Whiteoak & Green 1996). Contours start at 48 mJy beam^{-1} and increase inward in steps of 40 mJy beam^{-1} .

tio for SNRs in M33 (Smith et al. 1993, Gordon et al. 1998) show a very large scatter in the variation of this ratio with remnant size, making such an argument questionable (as also noted by Rosado et al. 1996). For the purpose of discussion here, we express the distance as $d_7 = (d/7 \text{ kpc})$ and scale all derived quantities accordingly.

Here we report on X-ray observations of G290.1–0.8 with the Advanced Satellite for Cosmology and Astrophysics (ASCA) in which we establish the thermal nature of the central X-ray emission and address the observed spectral and spatial characteristics. In Section 2 we discuss the observations and the results of the spectral analysis. We then investigate two scenarios to explain the X-ray characteristics: a cloudy ISM interpretation, using the similarity solution derived by White and Long (1991); and an SNR with thermal conduction interpretation, using a shock code to follow the evolution of model remnants until properties representative of those observed are achieved. Finally, we present a discussion of these results.

2. X-RAY OBSERVATIONS

G290.1–0.8 was observed with the ASCA observatory for 40 ks on March 1, 1994. Due to observation at small Earth angle, however, standard screening resulted in the rejection of a large fraction of the SIS data. A repeat observation was performed on January 16, 1995. The resulting SIS data were of somewhat reduced quality from that originally expected because of the degradation of the SIS detectors in 4-CCD mode.

The GIS image (0.5–10 keV) of G290.1–0.8 with radio contours from the MOST image (Whiteoak & Green 1996), is shown in Figure 2. Here the X-ray data have been smoothed with a 30 arcsec Gaussian followed by a background subtraction and vignetting correction. The boundary of the X-ray emission is strikingly similar to the radio boundary, but the morphology is centrally bright in X-rays while the radio emission shows no evidence of any enhancement associated with the bright X-ray center. The position of the peak X-ray emission is at roughly $\text{RA}_{2000}: 11^{\text{h}}03^{\text{m}}$, $\text{Dec}_{2000}: -60^{\circ}54'$.

X-ray images of composite SNRs (i.e. those containing a

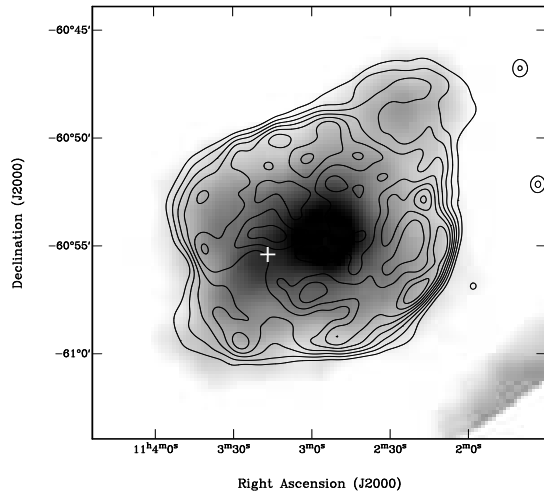


FIG. 2.— Background-subtracted, vignetting-corrected ASCA GIS image (0.5–10 keV) with radio contours from MOST. The point source observed in the ROSAT HRI is indicated by a cross.

central pulsar-driven synchrotron nebula) show distinct morphological differences above and below $\sim 1.5 \text{ keV}$, with the high energy tail of the power law spectrum from the centrally located synchrotron nebula dominating above 1.5 keV, where the thermal emission from the shell has fallen off (see Harrus, Hughes, & Slane 1997, Harrus & Slane 1998). We find no such energy dependence for the X-ray morphology of G290.1–0.8; the spectral characteristics appear relatively uniform over the remnant.

To determine the spectral properties, we have carried out joint spectral fits using the ASCA GIS and SIS data. For the GIS data we have used the outer regions of the detectors for extraction of background spectra. Use of blank-sky data for background, which were obtained at a high Galactic latitude (and thus do not include any contribution from the Galactic ridge emission in the direction of G290.1–0.8) yields similar results for the spectral analysis. Background for the SIS was taken from blank-sky fields.

All GIS2 and GIS3 data were merged to produce a single spectrum. In the earlier observation, the GIS3 data were taken with 128 bin spectral resolution in order to provide increased timing resolution. All GIS data were thus rebinned to this resolution before forming the joint spectrum; no loss of intrinsic instrument resolution is introduced in this process. A total of $\sim 55,000$ GIS events were obtained with a total effective integration time of 139 ks. The SIS data were also merged to form a joint spectrum yielding a total of $\sim 16,000$ events with an effective exposure of 52 ks.

The spectra (Figure 3) are roughly described by a thermal plasma in ionization equilibrium (Raymond & Smith 1977) with the addition of a weak power law component; the observed temperature is $kT \sim 0.5 \text{ keV}$ with an absorption in excess of 10^{22} cm^{-2} , and the fit yields a reduced χ^2 of 1.42. A gain adjustment of $\sim 2\%$ is required for the GIS data, a value which is within the uncertainties of the instrument calibration. The spectral fit is significantly improved with increased abundances for Mg, Si, and S, yielding a final reduced χ^2 of 1.02 for the spectral values shown in Table 1. The small hard com-

ponent ($\sim 2\%$ of the unabsorbed flux) may be an artifact of residual Galactic ridge emission, though we note that there is no evidence of iron-line features which typically characterize such emission (Yamauchi & Koyama 1993). Alternatively, this component could be associated with synchrotron emission from electrons accelerated by the SNR shock. Such a component is observed for a number of SNRs (e.g. Cas A, Tycho, Kepler, and others), including several (SN 1006, G347.3–0.5, and G266.2–1.2) for which such emission completely dominates the X-ray spectrum. In any case, the spectrum clearly establishes that the bright central X-ray emission is thermal in nature. Spectra taken in three annular regions surrounding the bright X-ray center show no strong evidence of spectral variability, although a small variation in the column density from region to region appears to be preferred by the spectral fits.

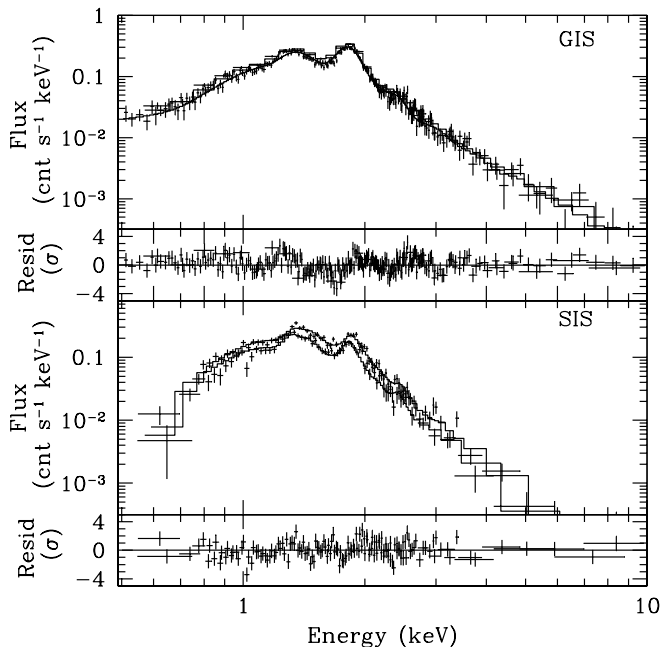


FIG. 3.— X-ray spectra from G290.1–0.8 from ASCA GIS and SIS. Histograms correspond to best-fit models as described in the text. Residuals for the fits are shown below each spectrum.

G290.1–0.8 was observed for ~ 15 ks with the ROSAT HRI on 29 January 1995. A faint source ($R = 5.6 \times 10^{-3} \text{ s}^{-1}$) is seen at $\text{RA}_{2000} = 11^{\text{h}}03^{\text{m}}19^{\text{s}}$, $\text{Dec}_{2000} = -60^{\circ}55'17''$ which is within ~ 3 arcsec of an unidentified 14th magnitude optical source, consistent with the position uncertainty in the HRI. The X-ray source is faint and does not contribute significant distortion to the overall brightness profile of the diffuse emission; its position is marked in Figure 2. There is no compact source of emission detected in the centrally enhanced region of the remnant.

3. INTERPRETATION

Having spectrally ruled out a central plerion scenario for G290.1–0.8, thus placing the remnant in the same class as W44 and other “mixed morphology” SNRs, we have considered two alternative scenarios for producing the observed center-filled X-ray morphology: evolution in a cloudy ISM (Cowie & McKee 1977; White & Long 1991), and an SNR for which thermal conduction effects have smoothed the temperature distribution. Below we discuss each case and compare the model predictions

with observed results from G290.1–0.8.

TABLE 1
SPECTRAL FIT PARAMETERS

| Parameter | Value ^a |
|----------------------------|--|
| N_H | $(1.3 \pm 0.1) \times 10^{22} \text{ cm}^{-2}$ |
| kT | $0.60 \pm 0.03 \text{ keV}$ |
| Abundance: | |
| Mg | 2.3 ± 0.3 |
| Si | 2.4 ± 0.3 |
| S | 1.4 ± 0.3 |
| $F_x(\text{thermal})^b$ | $1.8 \times 10^{-10} \text{ erg cm}^{-2} \text{ s}^{-1}$ |
| α | 1.4 ± 0.8 |
| $F_x(\text{nonthermal})^b$ | $2.2 \times 10^{-12} \text{ erg cm}^{-2} \text{ s}^{-1}$ |
| χ^2 | 578.3 (567 degrees of freedom) |

a) Uncertainties represent 90% confidence intervals

b) F_x = unabsorbed flux in 0.5 - 10.0 keV band

3.1. Cloudy ISM Model

The possibility that SNRs evolve in a two-phase ISM containing cold clouds embedded in a warmer diffuse intercloud medium was first discussed by Cowie & McKee (1977). In this scenario, the SNR blast wave rapidly passes the cold clouds leaving them relatively intact in the hot postshock gas. Here, through saturated conduction, they slowly evaporate and increase the central emission measure. White & Long (1991) developed a similarity solution for such evolution which incorporates two new parameters to the standard Sedov (1959) solution, namely C (the ratio of ISM mass in clouds to that in the intercloud medium), and τ (the ratio of the cloud evaporation timescale to the SNR age). For appropriate values of C and τ , centrally bright X-ray morphologies are possible.

To investigate the cloudy ISM scenario for G290.1–0.8, we constructed models covering a range of (C, τ) values. Using the emission measure derived from the GIS data, we varied the input shock temperature until the mean flux-weighted temperature for the model matched that derived from the data. We then constructed the radial brightness distribution for the model and compared it with the observed profile. The model surface brightness distribution was calculated from the model density and temperature distributions using emissivities for a plasma with abundances as derived from the spectral fitting. This was then folded through the observed interstellar absorption and the ASCA GIS and X-ray telescope spectral response, and the model brightness and temperature profiles were then compared with those derived from the GIS data. As illustrated in Figure 4, an adequate description of the data is obtained for (τ, C, kT_s) values between (10, 50, 0.49 keV) and (40, 150, 0.51 keV). While the brightness distribution differs somewhat from that observed (see further discussion in Section 4), the overall agreement is quite good for a spherically symmetric, homogeneous model; deviations of similar magnitude are typically encountered when attempting to fit profiles for shell-type remnants with ideal Sedov models. We note that the radio boundary indicated in Figure 4 is that of the most spherical component of G290.1–0.8, and this is the value used for the remnant radius in the (spherically symmetric) models. The apparent extension of the X-ray boundary beyond the radio shell is due primarily to the contribution from the extended regions of emission in the NW and SE (although the broad point spread of the telescope also smooths the outer X-ray boundary).

In Figure 5 we have plotted the derived properties of the remnant for (τ, C, kT_s) values of (10, 50, 0.49 keV). The depen-

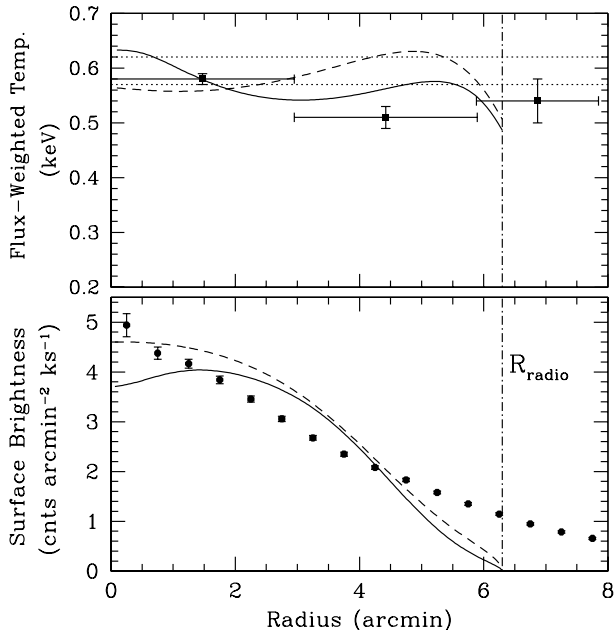


FIG. 4.— Comparison of cloudy ISM models with observed X-ray surface brightness and temperature profiles for G290.1–0.8. Points correspond to data from ASCA GIS observations. Curves correspond to models using the similarity solutions of White & Long (1991) for input parameters $(\tau, C, kT_s) = (10, 50, 0.49 \text{ keV})$ [solid] and $(40, 150, 0.51 \text{ keV})$ [dashed].

dence on assumed distance is shown explicitly. The derived value for the explosion energy ($\sim 3 \times 10^{50} \text{ erg}$) is somewhat low for the nominal $\sim 7 \text{ kpc}$ distance; more reasonable values ($\sim 8 \times 10^{50} \text{ erg}$) are obtained for a distance closer to $\sim 10 \text{ kpc}$, although we note that inferred explosion energies are often low with the W&L model (e.g. Harrus et al. 1997). Using the (τ, C, kT_s) values of $(40, 150, 0.51 \text{ keV})$ leads to a $\sim 50\%$ decrease in n_1 , but little change in the other derived quantities.

While the cloudy ISM model reproduces the observed X-ray characteristics of G290.1–0.8 quite well, an area of concern is the very long evaporation timescales (10 to 40 times the age of the remnant) required by the model. Models for evaporation of cold, dense clouds via saturated conduction predict relatively long evaporation timescales (McKee & Ostriker 1977). However, hydrodynamic simulations of shock/cloud interactions indicate that the clouds undergo considerable disruption (Stone & Norman 1992); models which require that cloudlets remain intact on timescales of many tens of thousands of years (as suggested by the values if τ) appear problematic. Magnetic fields may act to prolong the cloud destruction timescale (Mac Low et al. 1994) although this may also act to reduce the evaporation process because thermal conduction is heavily suppressed across magnetic field lines.

3.2. Thermal Conduction Model

In the later phases of SNR evolution, the shock front slows and becomes radiative, as the shocked material cools immediately after being heated. This occurs when the shock temperature falls below $\sim 0.1 \text{ keV}$, which, using the Sedov (1959) solution, corresponds to an age $t \sim 2 \times 10^4 (\frac{E_{51}}{n_0})^{1/3} \text{ yr}$, with a radius $R \sim 15 (\frac{E_{51}}{n_0})^{1/3} \text{ pc}$. After this stage, the X-ray emission above $\sim 1 \text{ keV}$ from the outer shell of the remnant effectively

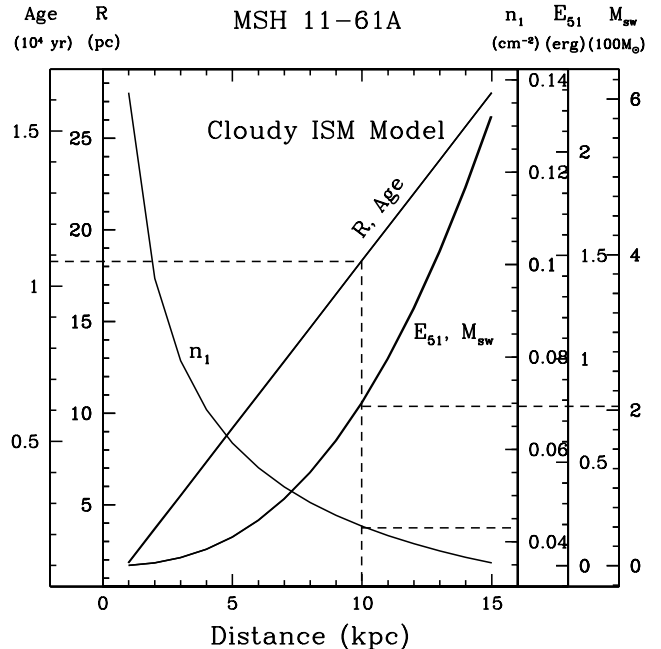


FIG. 5.— Derived parameters for G290.1–0.8 based upon cloudy ISM model. Curves for radius and age, E_{51} and M_{sw} , and n_1 are indicated with associated scales at left and right. Dashed lines indicate example values based upon a 10 kpc distance.

stops. In addition, the soft X-ray/EUV radiation from the radiative shock is readily absorbed, so the central hot region of the remnant dominates the X-ray emission.

In a pure Sedov solution, however, the temperature in the center of the remnant is extremely high, and the density low, so the total X-ray emissivity of the center will be very low as well. Reducing the central temperature and increasing the density would dramatically increase the emission. In the White & Long (1991) model, this moderation was achieved by assuming evaporating clouds exist inside the hot remnant. Another method is to include thermal conduction, via Coloumb collisions between the electrons and ions (Spitzer 1956), inside the hot plasma. This approach has been used to model the SNR W44 (Cox et al. 1999; Shelton et al. 1999), and to make models of the Local Bubble (Smith & Cox 2001).

We used a one-dimensional spherically symmetric Lagrangian shock code (ODIN) (Smith & Cox 2001) to model the temperature and density evolution of the SNRs into the radiative phase. ODIN calculates the non-equilibrium radiative cooling (using the 1993 version of the Raymond & Smith (1977) plasma emission model) from the hot plasma at each timestep. The electron and ion temperatures are assumed to be in equilibrium throughout. The magnetic field is assumed to be frozen in the plasma, and so contributes only to the pressure as a term $\propto n^2$. The thermal conduction model is based on Spitzer (1956), including the saturation limit from Cowie & McKee (1977). The code has been tested against the analytic Sedov model as well as the shock tube model (Smith 1996).

We constructed models for a range of (E, n_0) values and followed these to 50,000 years, by which time all had become radiative. We then calculated the NEI X-ray spectrum for each (E, n_0, t) point, folded this through the ASCA GIS

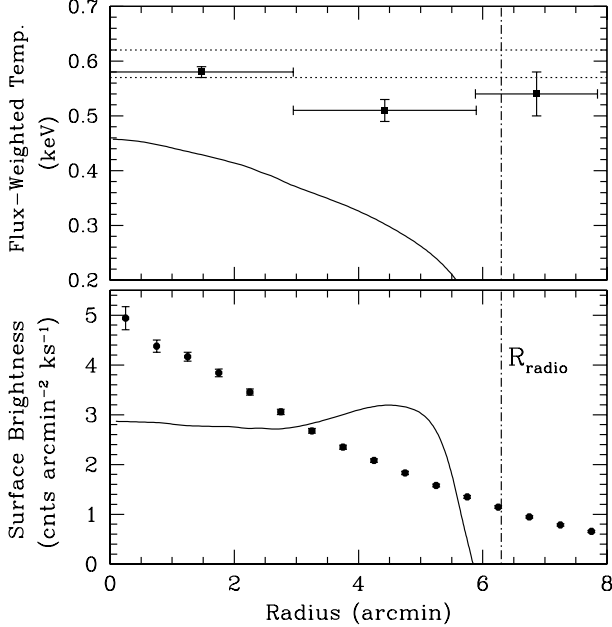


FIG. 6.— Comparison of thermal conduction model with observed X-ray surface brightness and temperature profiles for G290.1–0.8. Points correspond to data from ASCA GIS observations. Curves correspond to the thermal conduction model which best reproduces the average surface brightness and mean temperature of the remnant.

response, and found the predicted surface brightness. We restricted our search to those models that matched the observed surface brightness ($0.0025 \text{ GIS counts sec}^{-1} \text{ arcmin}^{-2}$). The temperature profiles of these models are all relatively flat compared to models without thermal conduction (*e.g.*, Sedov models). The central temperature is a function of ISM density n_0 but largely independent of supernova energy E , given the constraint on the surface brightness.

Since the observed temperature profile is quite flat at $\sim 0.6 \text{ keV}$, we were able to eliminate models with $n_0 \geq 2.0 \text{ cm}^{-3}$ because they were too cool throughout. Conversely, models with $n_0 \leq 0.5 \text{ cm}^{-3}$ were too limb-brightened. We were therefore driven to models with $n_0 = 1 \text{ cm}^{-3}$. In Figure 6 we show the flux-weighted temperature profile and the surface brightness for the model with $E_{51} = 1.0$ and $n_0 = 1.0 \text{ cm}^{-3}$. Clearly the flux-weighted temperature is systematically too low, although we note that the derived temperature is dependent upon the elemental abundances as well as the state of ionization equilibrium. We have modeled these parameters as well, but the important line features that are sensitive to the parameters are poorly constrained in broad-band fits to low spectral resolution data. The model surface brightness is also limb-brightened, in contrast to the centrally-peaked remnant morphology. Although the center of the remnant in this model has $kT > 0.7 \text{ keV}$, the emission from the edge dominates because the shock has not yet become radiative. It is important to note, however, that the limb brightness in this model is only $\sim 10\%$ higher than that for the remnant center, a condition far from that for a standard Sedov phase remnant. In Figure 7 we show the model results for the age, size, and explosion energy as a function of the assumed distance, for an ISM density of 1 cm^{-3} . Our models do predict the remnant age and radius as a function of explosion energy,

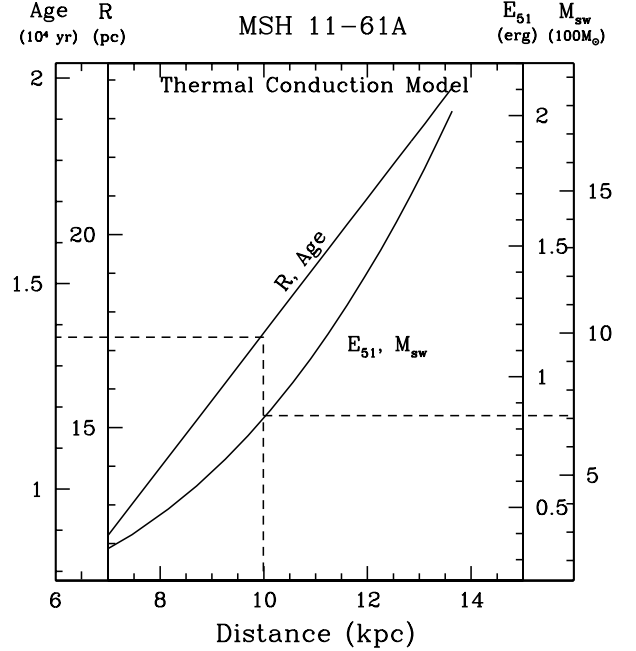


FIG. 7.— Derived parameters for G290.1–0.8 based upon radiative model with thermal conduction. Curves for radius, age, E_{51} and M_{sw} are indicated with associated scales at left and right. Dashed lines indicate example values based upon a 10 kpc distance.

but as the data do not constrain this parameter, we can report only ranges. For explosion energies $E_{51} = 0.3, 1.0, 2.0$, the remnant ages are 10, 16, and 22 kyr, and the radii 6.2, 9.6, and 12 pc, respectively.

4. DISCUSSION

Both of the models considered here yield X-ray emission that is centrally enhanced relative to that expected from a pure Sedov model. The observed brightness profile is actually steeper in the center than either model predicts, however, a situation that holds for similar modeling of W44 as well (Harrus et al. 1997, Shelton et al. 1999). One possible scenario to explain this could be the presence of ejecta in the central regions. The X-ray spectrum of G290.1–0.8 does show enhanced abundances of Mg, Si, and possibly Si, which could be consistent with this interpretation. However, there is currently no evidence that the measured abundance varies with radius, which would be required in such a scenario. Observations with higher angular resolution are of considerable interest in order to permit a more sensitive search for such spectral variations. We note that a second scenario which could modify the brightness profile in such a way as to boost the central emission might be evolution into a stellar wind density distribution. This would consist of a pre-existing density profile which declines rapidly with radius, thus yielding relatively more mass in the central regions. Incorporation of such profiles into the models discussed here is beyond the scope of this paper.

As illustrated in Figures 5 and 7, the derived properties for G290.1–0.8 differ for the two distinct models. However, the basic conclusion supported by each is that, for reasonable values of the explosion energy ($E_{51} \approx 0.5–1$), the remnant age is of order $(1–2) \times 10^4 \text{ yr}$, the distance is $\sim 8–12 \text{ kpc}$, and the amount

of swept-up mass is very large. G290.1–0.8 is clearly in the mid-to-late phase of evolution. Our thermal conduction models do not predict that the shock in G290.1–0.8 has gone radiative, unlike similar models used successfully for W44 (Shelton et al. 1999). This explains the slightly limb-brightened brightness profile for the model illustrated in Figure 6; it appears that thermal conduction models for mixed morphology SNRs only become centrally dominated in X-rays once the shock has become radiative. In the late phase of evolution, after the shock has become radiative, we expect the formation of a dense, thin outer shell that should be observable in HI. Such a shell is observed in W44 (Koo & Heiles 1995), for example, and HI observations of G290.1–0.8 are thus of considerable importance. We note that our thermal conduction models for G290.1–0.8 are unable to reproduce even the average surface brightness and mean temperature for cases where the shock is radiative. If HI observations do reveal a dense outer shell, this will imply that other parameters for the X-ray emitting plasma need modification if a thermal conduction model is to hold.

The X-ray characteristics of G290.1–0.8 can also be used to assess the likelihood of an association between the remnant and PSR J1105-610. The component of the pulsar velocity in the plane of the sky is given by $v_p = \beta D/t$ where D is the distance to the system, t is the age, and β is the angular separation (in radians) between the pulsar and the SNR center. From pulsar population studies, velocities are distributed in two roughly Gaussian components with characteristic speeds of 175 km s^{-1} and 700 km s^{-1} , representing 86% and 14% of the population, respectively (Cordes & Chernoff 1998).

For a remnant in the Sedov phase of evolution (including the case with evaporating clouds), the shock radius can be written

$$R_s = \left[\frac{25(\gamma+1)^2}{8(\gamma-1)} \frac{kT_s}{\mu m_H} \right]^{1/2} t$$

where T_s is the shock temperature, $\mu \approx 0.6$ for cosmic abundances, and $\gamma = 5/3$ for an ideal gas. Since $R_s = \theta D$, where θ is the angular size of the remnant, the pulsar velocity can be written

$$v_p = 6.8 \times 10^2 \left(\frac{\beta}{\theta} \right) T_6^{1/2} \text{ km s}^{-1}$$

where T_6 is the temperature in units of 10^6 K . For G290.1–0.8 we have $\theta \sim 6.3 \text{ arcmin}$, and PSR J1105-610 is located $\beta \sim 22 \text{ arcmin}$ from the remnant center. For the cloudy ISM model described above, the inferred shock temperature is $T_s = 4.1 \times 10^6 \text{ K}$. This leads to a pulsar velocity $v_p \approx 5.3 \times 10^3 \text{ km s}^{-1}$ which is much larger than expected for a true association between the two objects.

For the thermal conduction model, for which the Sedov solution no longer applies, the shock temperature is lower. Scaling the size/age relation from Figure 7 implies a pulsar velocity $v_p \approx 4.5 \times 10^3 \text{ km s}^{-1}$, still very large when compared with other pulsars. We conclude that G290.1–0.8 and PSR J1105-610 are unlikely to have been formed in the same supernova explosion.

5. CONCLUSIONS

The ASCA observations of G290.1–0.8 establish this remnant as another member of the “thermal composite” class whose X-ray morphology is dominated by thermal emission from the center. We have investigated two models in an effort to reproduce the observed temperature and brightness profiles. The cloudy ISM model based on the similarity solution by White & Long (1991) provides a reasonable description of these observed characteristics, and leads to a remnant of moderate age at a distance of $\sim 8\text{--}11 \text{ kpc}$ for explosion energies in the range $E_{51} = 0.5\text{--}1$. The required density of the intercloud medium is $\sim 0.4\text{--}0.05 \text{ cm}^{-3}$, and the cloud to intercloud mass ratio is of order 50–150. The evaporation timescale for the clouds is 10–40 times the age of the SNR, which may be problematic given that cloud-crushing timescales are typically much shorter than this. The observed brightness profile is more centrally peaked than the model predicts, which may indicate a need to consider a density profile modified by a precursor wind.

A hydrodynamic model which follows the remnant evolution toward the radiative phase, and incorporates the effects of thermal conduction, is also capable of increasing the central X-ray brightness and producing a somewhat flattened temperature distribution, but the brightness and temperature profiles differ considerably from those observed. It would appear that this model requires modifications to the ambient medium, and perhaps the ejecta component, in order to more closely reproduce the observed properties. The density required to reproduce the size and flux is $n_0 \sim 1 \text{ cm}^{-3}$, and the distance range associated with the explosion energy range used above is also $\sim 8\text{--}11 \text{ kpc}$.

With either of the above interpretations, the angular separation between G290.1–0.8 and PSR J1105-610 relative to the remnant radius implies a pulsar velocity much larger than that typical of even high velocity pulsars. This would suggest that PSR J1105-610 is not likely to be associated with the SNR if either of these interpretations for the evolution are correct.

This work was supported in part by the National Aeronautics and Space Administration through grants NAG5-3486 and NAG5-2638, and contract NAS8-39073. The authors would like to thank Ilana Harrus for many useful discussions on the nature of thermal composite SNRs.

REFERENCES

- Chen, Y. & Slane, P. 2001, *ApJ* - accepted for publication
 Cordes, J. M. & Chernoff, D. F. 1998, *ApJ*, 505, 315
 Cowie, L. L. & McKee, C. F. 1977, *ApJ*, 211, 135
 Cox, D. P. et al. 1999, *ApJ*, 524, 179
 Dickel, J.R. 1973, *Astrophys. Lett.*, 15, 61
 Elliot, K.H. & Malin, D.F. 1979, *MNRAS*, 186, 45
 Gaensler, B. M. 1998, *ApJ*, 493, 781
 Gordon, S. M., Kirshner, R. P., Long, K. S., Blair, W. P., Duric, N., & Smith, R. C. 1998, *ApJS*, 117, 89
 Goss, W.M., Radhakrishnan, V., Brooks, J.W., & Murray, J.D. 1972, *ApJS*, 203, 123
 Green D.A., 1998, ‘A Catalogue of Galactic Supernova Remnants (1998 September version)’, Mullard Radio Astronomy Observatory, Cambridge, United Kingdom (available on the World-Wide-Web at <http://www.mrao.cam.ac.uk/surveys/snr/s/>)
 Harrus, I. M., Hughes, J. P., Singh, K. P., Koyama, K., and Asaoka, I. 1997, *ApJ*, 488, 781
 Harrus, I. M., Hughes, J. P., & Slane, P. O. 1998, *ApJ*, 499, 273
 Harrus, I. M. & Slane, P. O. 1999, *ApJ*, 516, 811
 Harrus, I. M. Slane, P. O., Smith, R. K., & Hughes, J. P. 2001, *ApJ*, 552, 614
 Jones, L. R., Smith, A., & Angellini, L. 1993, *MNRAS*, 265, 631
 Kaspi, V. M., Bailes, M., Manchester, R. N., Stappers, B. W., Sandhu, J. S., Navarro, J., & D’Amico, N. 1997, *ApJ*, 485, 820
 Kirshner, R. P. & Winkler, P. F., Jr. 1979, *ApJ*, 227, 853
 Koo, B.-C & Heiles, C. 1995, *ApJ*, 442, 679

- Mac Low, M.-M., McKee, C. F., Klein, R. I., Stone, J. M. & Norman, M. L. 1994, *ApJ*, 433, 757
- McKee, C. F. & Ostriker, J. P. 1977, *ApJ*, 218, 148
- Raymond, J. C. & Smith, B. 1977, *ApJS*, 35, 419
- Rho, J.-H., & Petre, R. 1996, *ApJ*, 467, 698
- Rho, J.-H., & Petre, R. 1998, *ApJ*, 503L, 167
- Rosado, M., Ambrocio-Cruz, P., Le Coarer, E., & Marcelin, M. 1996, *A&A*, 315, 243
- Sedov, L. 1959, *Similarity and Dimensional Methods in Mechanics* (New York:Academic)
- Seward, F. D. 1990, *ApJS*, 73, 781
- Shelton, R. L. et al. 1999, *ApJ*, 524m 192
- Slane, P., Seward, F. D., Bandiera, R., Torii, K., & Tsunemi, H. 1997, *ApJ*, 485, 221
- Smith, A., Jones, L. R., Watson, M. G., Willingale, R., Wood, N., & Seward, F. D. 1985, *MNRAS*, 217, 99
- Smith R. K. 1996 - Ph.D. thesis, Univesity of Wisconsin
- Smith R. K. & Cox, D. P. 2001, *ApJS*, 134, 283
- Smith, R. C., Kirshner, R. P., Blair, W. P., Long, K. S., & Winkler, P. F. 1993, *ApJ*, 407, 564
- Spitzer, L. 1956, "Physics of Fully Ionized Gases", (New York: Interscience Publishers), p. 87
- Stone, J. M. & Norman, M. L. 1992, *ApJ*, 390, L17
- Vasisht, G., Aoki, T., Dotani, T., Kulkarni, S. R., Nagase, F. 1996, *ApJ*, 456, L59
- White, R. L. & Long, K. S. 1991, *ApJ*, 373, 543
- Whiteoak, J. B. Z. & Green, A. J. 1996, *A&AS*, 118, 329
- Yamauchi, S. & Koyama, K. 1993, *ApJ*, 404, 620